AGU PUBLICATIONS

Geophysical Research Letters

RESEARCH LETTER
10.1002/2017GL075495

Key Points:
- Tracking the life cycle of Integrated Water Vapor Transport (IVT) as "objects" provides unique empirical and descriptive data
- IVT objects typically exist five distinct regions, and their frequency of occurrence is strongly modulated by the AO, QBO, and PNA
- Results indicate that intense IVT objects are increasing globally by 3.58 events per year (95% confidence interval of ±1.39)

Supporting Information:
- Supporting Information S1

Correspondence to:
S. L. Sellars,
scottsellars@ucsd.edu

Citation:
Sellars, S. L., Kawzenuk, B., Nguyen, P., Ralph, F. M., & Sorooshian, S. (2017). Genesis, pathways, and terminations of intense global water vapor transport in association with large-scale climate patterns. *Geophysical Research Letters*, *44*, 12,465–12,475. https://doi.org/10.1002/2017GL075495

Received 18 SEP 2017
Accepted 4 DEC 2017
Accepted article online 8 DEC 2017
Published online 26 DEC 2017

Genesis, Pathways, and Terminations of Intense Global Water Vapor Transport in Association with Large-Scale Climate Patterns

S. L. Sellars[1], B. Kawzenuk[1], P. Nguyen[2], F. M. Ralph[1], and S. Sorooshian[2]

[1]Center for Western, Weather, and Water Extremes, Scripps Institute of Oceanography, La Jolla, CA, USA, [2]Center for Hydrometeorology and Remote Sensing, University of California, Irvine, Irvine, CA, USA

Abstract The CONNected objECT (CONNECT) algorithm is applied to global Integrated Water Vapor Transport data from the NASA's Modern-Era Retrospective Analysis for Research and Applications – Version 2 reanalysis product for the period of 1980 to 2016. The algorithm generates life-cycle records in time and space evolving strong vapor transport events. We show five regions, located in the midlatitudes, where events typically exist (off the coast of the southeast United States, eastern China, eastern South America, off the southern tip of South Africa, and in the southeastern Pacific Ocean). Global statistics show distinct genesis and termination regions and global seasonal peak frequency during Northern Hemisphere late fall/winter and Southern Hemisphere winter. In addition, the event frequency and geographical location are shown to be modulated by the Arctic Oscillation, Pacific North American Pattern, and the quasi-biennial oscillation. Moreover, a positive linear trend in the annual number of objects is reported, increasing by 3.58 objects year-over-year.

Plain Language Summary A computational science approach to tracking global atmospheric water vapor plumes is applied to a NASA data set from 1980 to 2016. Results show regions of the globe where intense water vapor transport often exists, including their genesis and termination locations. Winter time months tend to have more water vapor plumes in both the Southern and Northern Hemispheres. In addition, climate phenomena also have an impact on the frequency and location of these water vapor plumes.

1. Introduction

Large-scale water vapor transport processes in the atmosphere are an important component of the global hydrological cycle (Waliser & Guan, 2017). Water vapor transport is driven by different mechanisms in the atmosphere, including midlatitude, extratropical cyclones, tropical cyclones, and monsoon transport. In the midlatitudes, one phenomenon known to transport massive amounts of water vapor globally, and the primary focus of this paper, is atmospheric rivers (ARs). An AR is defined as "a long, narrow, and transient corridor of strong horizontal water vapor transport that is typically associated with a low-level jet stream ahead of the cold front of an extratropical cyclone" (American Meteorological Society, 2017). In recent years, ARs have been found to be major contributors to extreme rain events leading to flooding, mudslides, and other natural hazards impacting the western U.S. (Dettinger et al., 2011; Neiman et al., 2013; Ralph & Dettinger, 2011; Ralph et al., 2006, 2011; Ruby Leung & Qian, 2009; White et al., 2013, among others). In addition, ARs have been found to have beneficial impacts such as contributing to water resources and mitigating and breaking droughts (Dettinger, 2011, 2013; Guan et al., 2010). The frequency, location, and landfall of these extreme rain events associated with ARs have been shown to be modulated by season, geographic region, and climate variability (Baggett et al., 2017; Guan et al., 2012; Guan & Waliser, 2015; Mundhenk et al., 2016; Sellars et al., 2015; Waliser & Guan, 2017).

Scientists are interested in understanding ARs' occurrences, including their frequency, landfall location, and intensity. One of the challenges in studying ARs is defining the event, given that ARs are highly dynamic and fluid areas of the atmosphere and are notoriously challenging to track in time and space. Similar challenges have been observed when tracking other atmospheric phenomena, including tropical cyclones (Ullrich & Zarzycki, 2017; Kerns & Zipser, 2008, 2009) and extratropical cyclones (Hodges et al., 1994). Many methods have been developed and used to characterize AR events into catalogs, or list of dates when ARs occur at specific locations. These AR detection methods are regional and global

(Dettinger, 2011; Hagos et al., 2015; Mundhenk et al., 2016; Neiman et al., 2009; Ralph et al., 2012; Rutz et al., 2014; Sellars et al., 2013, 2015; Wick et al., 2013) and provide researchers with the means to study the statistical information impacting their formation and evolution.

AR detection methods often focus on one or two variables, Integrated Water Vapor (IWV) (Hagos et al., 2015; Jiang et al., 2014; Neiman et al., 2008; Ralph et al., 2004; Wick et al., 2013) or Integrated Water Vapor Transport (IVT), which were shown to be fundamental components of ARs (Moore et al., 2012; Neiman et al., 2008; Rutz et al., 2014). Ralph et al. (2004) focused on using remotely sensed observations of IWV to isolate the AR structure. They defined ARs as a continuous region of at least 20 mm of IWV that were at least 2,000 km in length and less than 1,000 km in width. Other detection approaches advanced using strict geometrical criteria (Guan et al., 2015; Lavers et al., 2013; Mundhenk et al., 2016; Rutz et al., 2014). It is important to note that these previous studies do not focus on tracking ARs as unique objects over their entire life cycle, they simply seek to determine if an AR is present at a given time or location, based on the criteria described above.

To address limitations and lack of life-cycle tracking by current AR catalogs and to capture other water vapor transport mechanisms important in global water vapor transport (e.g., tropical cyclones and monsoons), this study isolates IVT transport events without setting any geometrical or percentile-based criteria by introducing a tracking algorithm that has advanced data structure: the CONNected objeECT, or CONNECT algorithm (Sellars et al., 2013, 2015). One advantage of the CONNECT algorithm is that it keeps track of the entire life cycle of an object, from the genesis to the termination location by "connecting" pixels in time and space, and tracking the system to be analyzed as a "4-D" object. These objects can originate from any location and propagate globally and can be continuously tracked.

This study harnesses the CONNECT approach to build global life-cycle records of the time and space of evolving IVT objects from their genesis to termination, track climate conditions, and determine how climate variability impact their characteristics. The National Aeronautics and Space Administration (NASA) Modern-Era Retrospective Analysis for Research and Applications (Bosilovich et al., 2011; Gelaro et al., 2017; Rienecker et al., 2011), Version 2 (MERRA V2) is used from 1980 to 2016. From this point on, the archive is referred to as IVT-CONNECT (Sellars et al., 2017). To investigate climate variabilities' impact on IVT objects, the population of objects contained in the archive were split into subsets during the positive/negative (±) phases of one global index, the quasi-biennial oscillation (QBO) (Baldwin et al., 2001), and two regional climate indexes, the Arctic Oscillation (AO) (Thompson & Wallace, 1998) and the Pacific North American Pattern (PNA) (Barnston & Livezey, 1987).

2. Materials and Methods

2.1. CONNected objECT (CONNECT) Tracking Algorithm and Data

The four-dimensional (4-D) object-oriented algorithm was developed by a team of researchers from the University of California, Irvine (Sellars et al., 2013, 2015). Earth science variables can be described as statistical 4-D objects evolving in space (2-D), time (1-D), and magnitude of the selected variable (IVT in this case) (1-D). The algorithm defines objects by identifying instantaneous IVT "footprints" (i.e., the geographic spatial patterns) and recognizes the sequential footprints from the same system with overlapped or "connected" areas in time and space. Each object has a unique ID and set of selected characteristics. Figure S1 in the supporting information shows the time evolving footprint of a single IVT object over its life cycle. The time and space footprint represents the dynamical evolution of the phenomena and can be associated with weather and climate features (e.g., midlatitude jet stream and ocean/atmosphere teleconnections). Organizing the data into 4-D objects helps one to visualize the dynamical changes to the object (iRain-UC Irvine, 2017; Nguyen et al., 2017).

The MERRA V2 reanalysis product represents the satellite era using a state-of-the-art assimilation system, known as the Goddard Earth Observing System Data Assimilation System Version 5 (Bosilovich et al., 2015; Rienecker et al., 2011). The data have a temporal frequency of 3-hourly from 00:00 UTC (instantaneous), with a 3-D spatial grid at full horizontal resolution. The resolution is 0.5° × 0.625° in latitude and longitude, and 42 vertical levels from the surface to 0.01 hPa. For the calculation of IVT, the assimilated meteorological field data archive (M2I3NPASM) is used.

2.1.1. Integrated Water Vapor Transport

IVT is a measure of the horizontal water vapor transport in the atmosphere integrated from 1,000 to 200 hPa calculated from several parameters available in the MERRA data set. The IVT is calculated similar to the methodology of Cordeira et al. (2013) and is defined as

$$\mathrm{IVT} = -\frac{1}{g}\int_{1000\ \mathrm{hPa}}^{200\ \mathrm{hPa}} qV dp$$

where q is the specific humidity, g is the gravitational acceleration, and V is the total vector wind. The units for IVT are kilograms of water per meter per second, and the vertical integration is computed using 25 hPa isobaric layers from 1,000 to 700 hPa and 50 hPa layers from 700 to 200 hPa.

2.1.2. CONNECT Algorithm Settings for MERRA-V2's IVT Data

CONNECT requires two thresholds: (1) a minimum value of the selected variable to locate intensity patterns or "footprints" with a certain magnitude and (2) a life-cycle time threshold that ensures the object exists for a minimum length in time. To generate IVT-CONNECT, the study set a minimum threshold of IVT intensity at 750 kg m^{-1} s^{-1} and applied a duration threshold that required all systems to have a life cycle of at least 24 h (i.e., ignoring systems that last for a shorter time periods under these conditions). Twenty-four hours was found to be a good temporal threshold for segmenting large-scale atmospheric systems as reported in Sellars et al. (2015). Midlatitude water vapor transport studies associated with ARs have used a threshold as low as 250 kg m^{-1} s^{-1} and if used herein would include weak to moderate transport processes. The 750 kg m^{-1} s^{-1} threshold is selected to target only the strongest water vapor transport processes. There is a sensitivity of the results to the choice of the IVT threshold, as with all AR detection methods, but further discussion is beyond the scope of this paper.

2.2. IVT-CONNECT Physical and Climate-Based Features

Each object that has been generated by the CONNECT algorithm can be described using a wide range of features (i.e., descriptors of the object). For the physical features, the genesis and termination regions can be determined using the first and final groupings of pixels for each object in the data set. Other physical features include duration, average intensity, speed (km/h based on the distance change between centroid locations from sequential time steps), and many others that can be seen in Table S1 in the supporting information.

Similar to the physical based features, each object can be described by the phase of specific climate phenomena that existed when the object occurred. This paper focuses on only three large-scale climate phenomena described as features below, AO, QBO, and PNA, and were downloaded from the National Oceanic and Atmospheric Administration. Many other features are calculated but are beyond the scope of this paper (see Table S1).

2.2.1. Arctic Oscillation (AO)

The Northern Annular Mode, or Arctic Oscillation (AO), is a major cause of extratropical circulation variability in the midlatitude and high latitude of the Northern Hemisphere (NH). AO is characterized by a zonal symmetry of the north-south geopotential height perturbations impacting the midlatitude jet stream (Thompson & Wallace, 1998). The loading pattern of AO is defined as the first leading mode from the principle component analysis of monthly mean height anomalies at 1,000 hPa (NH) or 700 hPa (SH). The seesaw pattern (positive and negative phase) describes the strength and location of the geopotential height perturbations and can allow arctic air to penetrate the middle latitudes causing short-medium shifts in regional climate.

2.2.2. Quasi-Biennial Oscillation (QBO)

The QBO is described as the prevailing eastward and westward propagation of winds in the equatorial stratosphere at approximately 16 to 50 km above the Earth's surface. The wind jets quasi-biennially descend through the stratosphere from near the top of the atmosphere, ~1 hPa, down to the top of the troposphere ~100 hPa (Baldwin et al., 2001; Ebdon, 1960; Lindzen & Holton, 1968). The QBO is considered a tropical phenomenon, as the vertical wave propagation originates there; yet, it is known to affect the stratospheric flow in the polar regions thus modulating extratropical wave propagation (Baldwin et al., 2001). Here the QBO index is calculated from the zonal average of the 30 hPa zonal wind at the equator as computed from the National Centers for Environmental Prediction/National Center for Atmospheric Research Reanalysis, where eastward and westward propagation is characterized by negative and positive values, respectively.

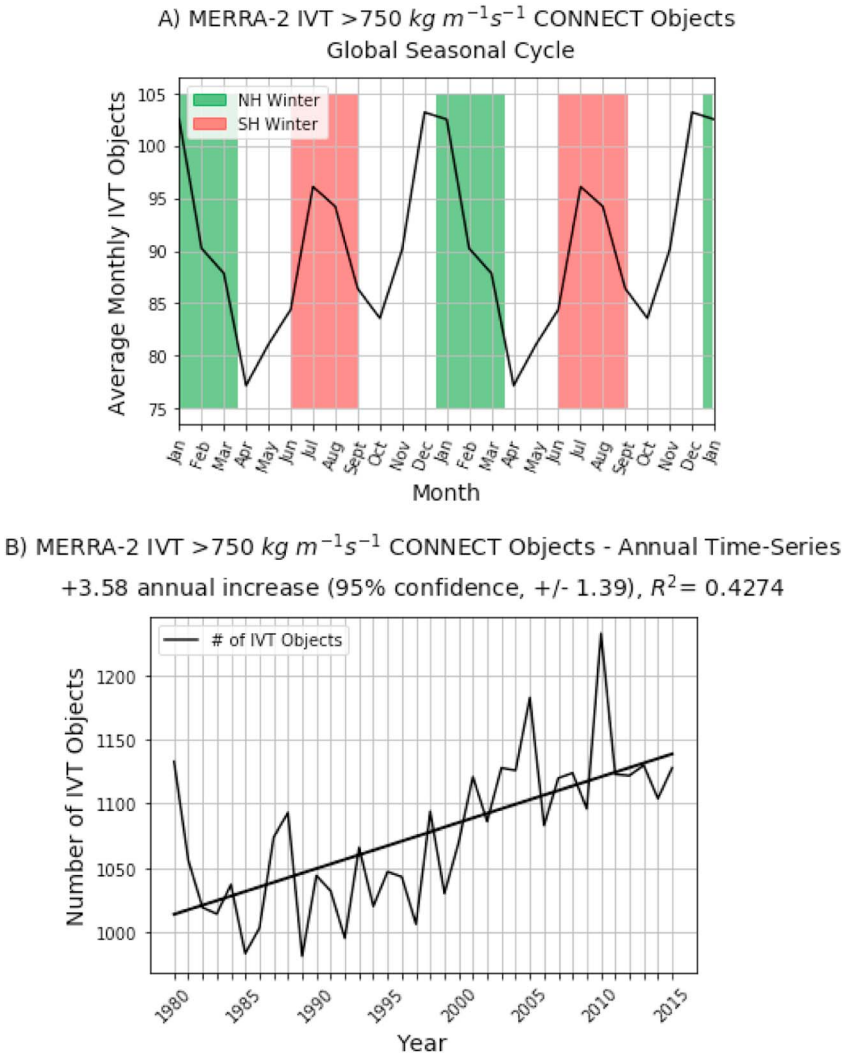

Figure 1. (a) Global IVT-CONNECT object average monthly values (i.e., seasonal cycle—repeated once for visualization). (b) Global IVT-CONNECT object annual frequency with linear trend overlaid.

2.2.3. Pacific North American Pattern (PNA)

The PNA is a phenomenon known to influence North American climate, consisting of anomalies in midtropospheric geopotential height over the U.S. The PNA is calculated using the orthogonally rotated principle component analysis of 1 month mean NH 700 hPa heights. The PNA leading patterns show a dipole with two phases; a positive phase of above normal geopotential-heights (higher pressure) over the western U.S., and below normal geopotential-heights (lower pressure) over the eastern U.S, and a negative phase with the opposite pattern of below normal heights over the western U.S. and above normal heights over the southeastern U.S. (Barnston & Livezey, 1987; Latif & Barnett, 1994).

3. Results

3.1. Global IVT-CONNECT Object Climatology

The IVT-CONNECT data set has a total of 39,480 objects globally. The objects are independent in the sense that they are not directly connected to one and another in time or space. Analyzing annual and monthly counts of objects provide insight into global characteristics of the monthly, seasonal, and interannual frequency of the events. Annual and monthly mean frequency results are 1,067 and 89.7 objects, respectively. The seasonal cycle and interannual variability are shown in Figure 1a, which shows two peaks in the seasonal

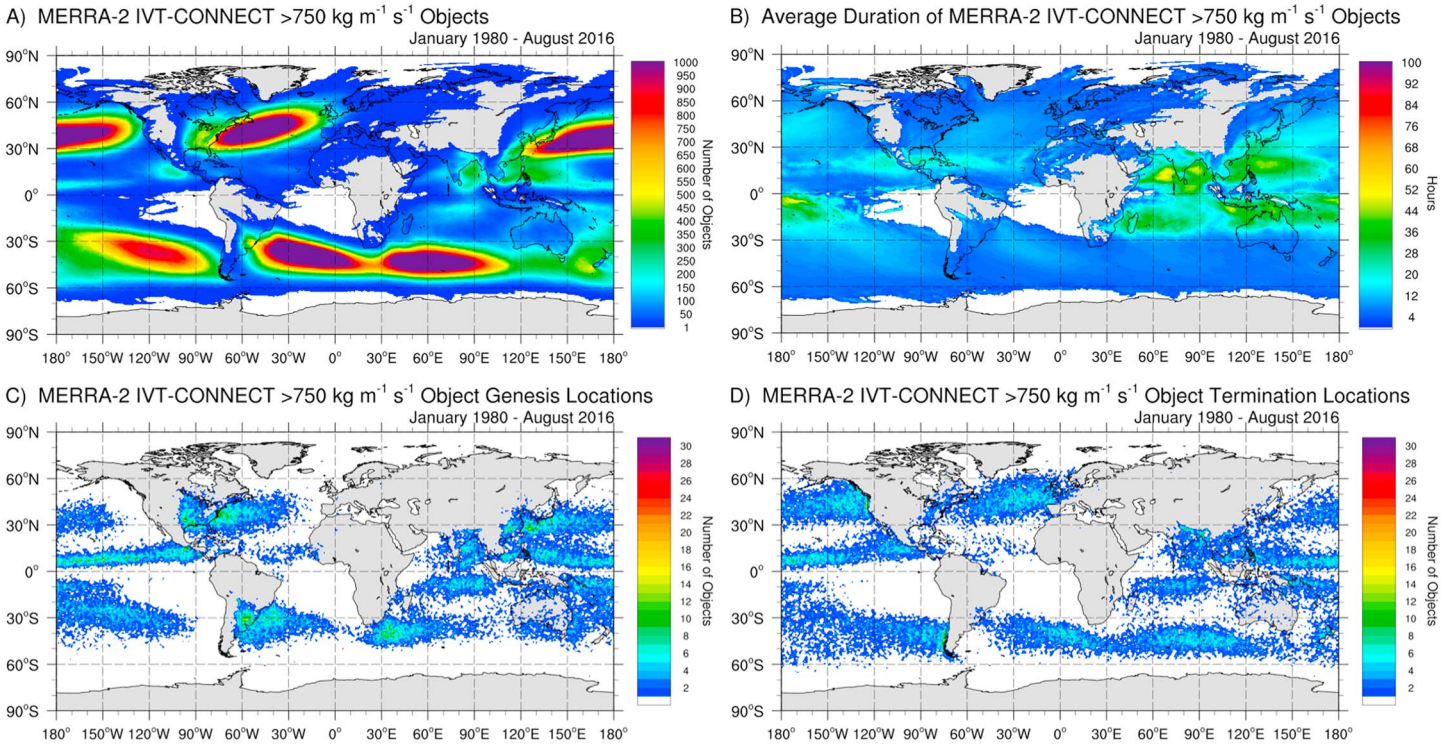

Figure 2. (a) Total number of IVT objects from January 1980 to August 2016. (b) Average duration in hours of object at each grid cell. (c) The number of objects at genesis (starting) locations for all IVT objects. (d) The number of objects at termination (ending) locations for all IVT objects. The gray areas represent landmass.

cycle. One peak is in NH late fall and SH late spring (November/December), and the second peak is during NH summer/SH winter (July/August). These results indicate that the pole to equator temperature gradient and solar radiation maxima/minima, and the resulting seasonal shifts in large-scale atmospheric circulation (e.g., shifting of the midlatitude jet stream), for each hemisphere may play a role in IVT object genesis. The annual number of objects for the period 1980 to 2016 is shown in Figure 1b, with a range of annual IVT objects from 981 to 1,233. An increasing trend is observed with an estimated linear increase of 3.58, corresponding to a 95% confidence interval of ±1.39, year-over-year for the recorded period (with the baseline 1,067 per year on average). These results indicate the influence that global climate trends may have on IVT object genesis and will be detailed in additional research.

3.2. Global IVT-CONNECT Object Locations

An investigation of the IVT object locations revealed distinct regions where IVT "seed" regions exist. There is a large-scale organization of IVT objects globally with broad hemispheric patterns, spanning the Pacific and Atlantic Ocean basins in both hemispheres and tend to be located in the midlatitude regions. Figure 2a highlights five regions (off the coast of the southeast United States, eastern China, eastern South America, off the southern tip of South Africa, and the over the ocean in the southeastern Pacific) that have the largest number of objects, in terms total number of objects to impact each grid cell. IVT objects tend to be over the extratropical ocean basins, propagating eastward and oriented toward the poles; similar results were found in Zhu and Newell (1994, 1998) and Guan and Waliser (2015). The most pronounced regions lie to the east of continental landmasses (Asia, North America, and South America), with two regions that originate over the ocean (southern tip of Africa and southeastern Pacific Ocean).

A geographical assessment concludes that the two NH regions, off the coast of East Asia and eastern U.S., are known to include moisture-rich sources, such as dense vegetation and high tropical atmospheric moisture. Tropical systems tend to move westerly and can recurve northward and eastward when encountering the prevailing westerly winds in the subtropics. Intense moisture anomalies are known to propagate northward, along the Gulf of Mexico, and have been linked to IVT anomalies causing floods in the central U.S. (Lavers &

Villarini, 2013; Moore et al., 2012). Depending on the large-scale atmospheric circulation patterns, anomalous moisture can propagate northeasterly across the southeastern U.S., moving offshore toward the northern Atlantic, impacting Europe (Ramos et al., 2016). A similar mechanism often occurs east of Asia as tropical systems often recurve and undergo extratropical transition and transport large amounts of moisture across the north Pacific (Jones et al., 2003).

The IVT object seed regions in the SH include the east coast of South America, South Pacific, and southern Indian ocean. The dynamics of the South American jet stream, influenced by the Andes Mountain range and rainforest moisture to the east, prove to be incredibly conducive to the formation of IVT objects off the east coast of South America as the topography can promote the growth of atmospheric wave perturbations and lee cyclogenesis (Gan & Rao, 1991; Vera et al., 2002). Off the southern tip of South Africa is also a key IVT object formation region. Hoskins and Hodges (2005) shows similar regions of "storm" genesis downstream of the Andes and off the Southern tip of South Africa. The southeastern Pacific Ocean also shows increased objects between 30°S and 60°S. Nguyen et al. (2017) recently showed the South Pacific being influenced by barotropic wave train patterns from Hadley Circulation (HC) extension into the midlatitudes and extratropics of the SH. This HC extension is seen when tropical heating in the Indian Ocean-Maritime Continent region occurs and it is plausible that IVT spatial orientation and frequency are also related to this mechanism.

3.3. Global IVT-CONNECT Object Average Duration

IVT-CONNECT object average duration is calculated at each grid cell and represents the average number of hours (based on 3-hourly time steps) for all unique objects impacting that cell (Figure 2b). The longest duration IVT objects tend to be in the tropical region, between −30°S and 30°N with an average of 16.2 h. The monsoon regions (such as the Indian Monsoon and over the Maritime Continent) show this increased duration, suggesting that these large-scale moisture transport processes are important when considering intense IVT globally. These tropical regions feature a lower number of IVT-CONNECT objects than the midlatitudes (Figure 2a); however, when they do occur the duration is significantly longer.

The IVT object storm tracks in the midlatitudes are shown extending across the ocean basins with a lower midlatitude average duration of 8.8 h from 30.5°N to 60°N and 7.2 h from 30.5°S to 60°S. This is in contrast with the AR duration results shown in Guan and Waliser (2015), where they found the longest durations existed in the extratropical ocean basins at 16 h. This difference is most likely caused by several factors included in the detection methods. First, they apply geometric constraints that restrict ARs to have a long and narrow shape; second, the threshold used was the 85th percentile value of IVT, which is much lower than 750 kg m^{-1} s^{-1} used in this study, resulting in significant differences in duration.

3.4. Global IVT-CONNECT Object Genesis and Termination Locations

The genesis and termination locations of each IVT-CONNECT object are shown in Figures 2c and 2d. For visualization purposes these locations are displayed rounded to the nearest one degree. Several distinct regions appear as the main genesis locations for the objects with the majority appearing near ~10°N or 30°N or S. Midlatitude genesis regions are most likely associated with extratropical cyclones and/or ARs, while tropical genesis regions are most likely associated with tropical cyclones, strong convection, or monsoon patterns. The highest number of genesis points are in general upstream of regions with the highest number of objects (Figure 2a), suggesting that most IVT-CONNECT objects are not stationary and propagate along the large-scale atmospheric flow. The grid point with the highest number of object genesis is over the Gulf of Tehuantepec, central America. This is most likely due to the topography of the region as the Chivela Pass is a low-lying gap in the otherwise high topography of the Sierra Madre Mountain ranges. Given the right large-scale atmospheric environment, strong gap-outflow winds can be generated in this region and penetrate over the eastern Pacific (Schultz et al., 1997; Steenburgh et al., 1998).

The termination locations show enhanced clusters of landfall locations on the west coast of continents (Figure 2d). These regions of high terminations in most cases, and especially in the midlatitudes, appear downstream from the highest concentrated genesis regions. Key locations include the western U.S., western Europe, and southwest South America. Many studies have found the western U.S. (Rutz et al., 2014) and western Europe (Lavers et al., 2012) to be regions with elevated IVT often associated with landfalling ARs during

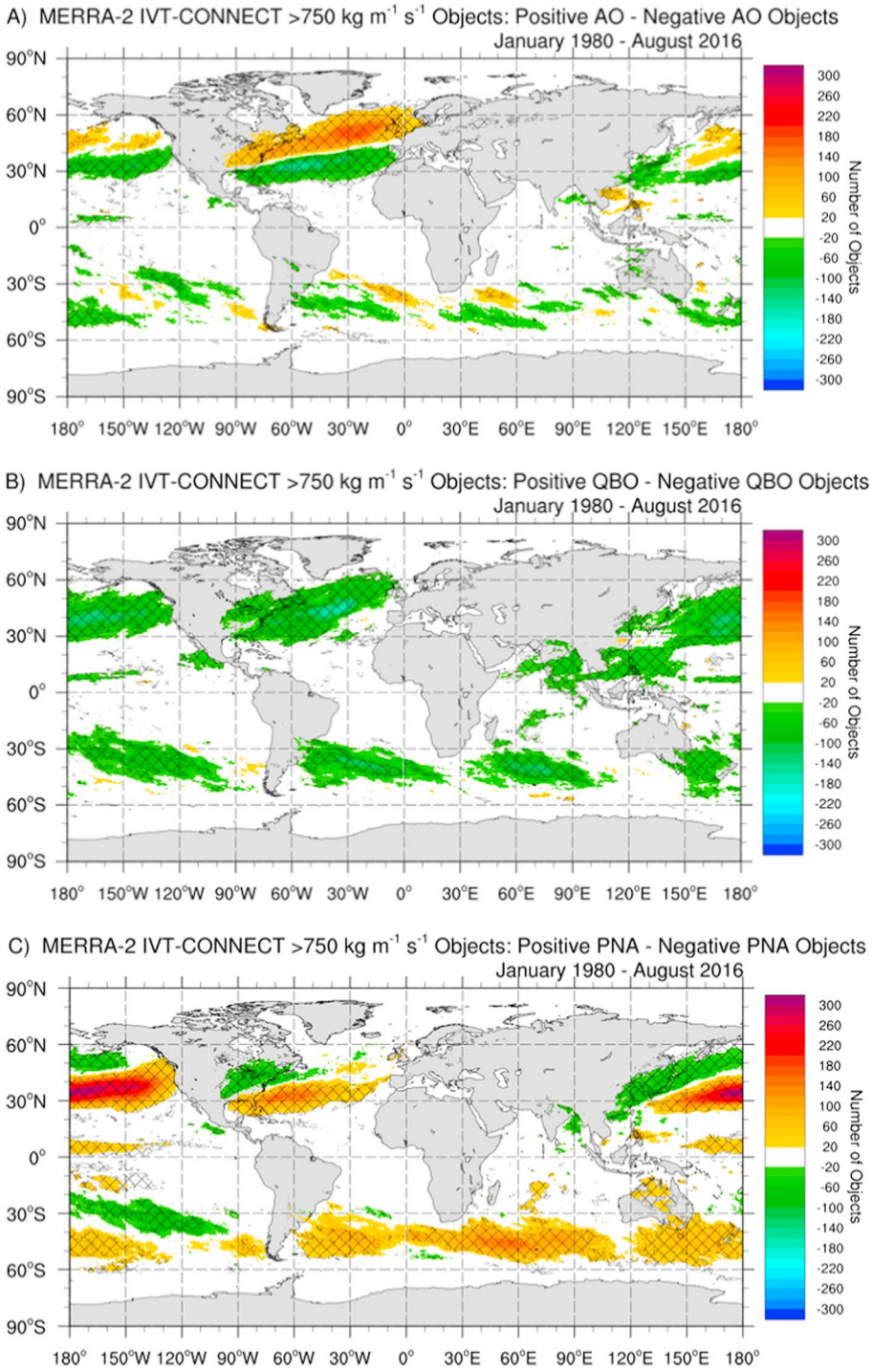

Figure 3. (a) Total number of positive (+) AO minus negative (−) AO IVT objects. (b) Total number of positive (+ or westerly phase) QBO minus negative (− or easterly phase) QBO IVT objects. (c) Total number of positive (+) PNA minus negative (−) PNA IVT objects. Hatching indicates regions where the difference between the total number of objects categorized by climate phase are statistically significant based on Fisher's Exact Test with p-value $< .01$. Background gray shading represents land masses.

the cool season. Other studies have documented AR landfalls in the central Andes in South America (Vera et al., 2002; Viale & Nuñez, 2011; Viale et al., 2013). North of 60°N and south of 60°S, fewer intense IVT objects occur, although it should be noted that it is not zero. AR landfalls do occur in high latitudes, such as Greenland and Antarctica, and are active area of research (Gorodetskaya et al., 2014; Neff et al., 2014);

however, most ARs in these regions do not reach IVT values of 750 k m^{-1} s^{-1} due to the limited moisture holding capacity of air at cooler temperature.

3.5. Global IVT-CONNECT Objects: Large-Scale Climate Variability Impacts

Using the IVT-CONNECT data set, groupings of objects can be easily performed using different phases of climate indicators. Figure 3a shows the difference in the number of objects that occurs between AO+ phase and AO− phase (based on NOAA's AO PC EOF1 PSL time series statistical index), where the difference in number of objects in these two phases is displayed as colored contours. Positive values represent locations where more IVT-CONNECT objects occurred in the positive phase than in the negative phase. In the North Atlantic and North Pacific oceans, the IVT objects associated with the positive or negative AO phase show a distinct shift in location and spatial orientation. Objects during a positive (negative) AO phase showed a more northerly (southerly) track and were predominately north (south) of ~40°N. Many studies have indicated how the AO can modulate the geopotential height field and thus shift the storm track (Lorenz, 1951; Thompson & Wallace, 2000a, 2000b) in the NH midlatitudes. In addition, Jeong and Ho (2005) showed enhanced penetration of cold Arctic air and associated storminess over the North Atlantic during the negative AO phase.

Recent studies have shown that the negative phase of QBO is generally driven by upward propagating tropical waves, and the frequency of these upward propagating waves can increase the midlatitude waves from the tropics, including teleconnections to the Madden Julian Oscillation, known to modulate extratropical weather and climate (Hood, 2017; Son et al., 2017). Figure 3b compares the number of IVT-CONNECT objects that occurred at each grid point during positive and negative QBO phases. In most locations, globally more IVT-CONNECT objects occurred during the negative phase. This pattern is especially evident in the NH midlatitude storm tracks over the north Atlantic and Pacific oceans between 30°N and 50°N. These regions saw significant increases in IVT-CONNECT objects during the negative QBO phase. Baggett et al. (2017) found anomalous IVT values point toward the Pacific Northwest, which suggests higher (lower) likelihood of AR landfalls during the −QBO (+QBO) as well.

Leathers et al. (1991) described the correlation between midtropospheric flows associated with each PNA phase and the resulting precipitation over North America. It was shown that a more zonal flow associated with the −PNA phase will result in the polar jet being pushed further north over the eastern U.S. Similar results were found by Coleman and Rogers (2003), who found that the PNA index is strongly aligned to water vapor transport in the Ohio Valley. This mechanism is highlighted in the spatial orientation and increased frequency of IVT-CONNECT objects associated with a −PNA over the northeast U.S. (Figure 3c). The opposite of this mechanism, +PNA, results in more development of IVT-CONNECT objects over the southeastern U.S. and offshore of the western U.S. A significant shift in storm track over the north Pacific is also observed.

4. Conclusions

In this paper, CONNECT is applied to MERRA-V2 IVT data to provide a global climatological record of life cycle, time, and space evolving IVT-CONNECT objects, including their genesis and termination regions. Each IVT-CONNECT object is described by physical and environmental characteristic information. These data were used to investigate geographical regions where IVT objects exist and large-scale climate variability is shown to impact the dynamics of water vapor transport, spatial orientation, and frequency of occurrence.

Thirty-nine thousand, four hundred, and eighty IVT-CONNECT objects were detected and tracked over their life cycle. IVT objects exist globally and show broad hemispheric patterns in five distinct regions. These results agree with foundational work by Zhu and Newell (1994) that midlatitude transport of moisture tends to be over the extratropical ocean basins, propagating eastward and oriented toward the poles. IVT object subsets provide the ability to investigate different physical and environmental characteristics from three selected climate phenomena, AO, QBO, and PNA. Results show that IVT object frequency and location are modulated depending on the phase of each phenomena. Through additional research and analysis of object frequency and features, it may be possible to use this tool to determine causality by building predictive models that accurately predict IVT object frequency based on these results.

CONNECT can be applied to any Earth science variable (i.e., sea surface temperature, sea level pressure, and atmospheric vorticity) for object analysis. This tool will allow these future studies to investigate other modes

of variability and climate features in the Earth system, some of which are shown in Table S1 in the appendix. Further research will continue to investigate the connection between moisture transport processes and large-scale climate dynamics, with the hope that insight can be gleaned about the causes of the mechanisms found and patterns that exist. Exploration of the interconnectivity of Earth system phenomena and physical and environmental features using CONNECT is unlimited.

Acknowledgments
The authors would like to thank UC San Diego Qualcomm/Calit2's John Graham and Pacific Research Platform (ACI-1541349) for supporting the PRP/CONNECT pilot project with network data transfer and storage support. This research was partially supported by the Department of Energy (DE-IA0000018), California Energy Commission (300-15-005) and California Department of Water Resources (4600010378) US Army Corps of Engineering (ICIWaRM and W912HZ-15-2-0019), UNESCO's G-WADI program, and National Science Foundation (1331915). The authors would like to also thank Cory Baggett, Elizabeth Barns, and Dan Cayan for the insightful discussions. Data are achieved and available at the UC San Diego Library's Research Data Curation Program (https://doi.org/10.6075/J01834P8).

References

American Meteorological Society (2017). Atmospheric River. Glossary of Meteorology. Retrieved from http://glossary.ametsoc.org/wiki/Atmospheric_river

Baggett, C. F., Barnes, E. A., Maloney, E. D., & Mundhenk, B. D. (2017). Advancing atmospheric river forecasts into subseasonal-to-seasonal time scales. *Geophysical Research Letters*, *44*, 7528–7536. https://doi.org/10.1002/2017GL074434

Baldwin, M. P., Gray, L. J., Dunkerton, T. J., Hamilton, K., Haynes, P. H., Randel, W. J., … Takahashi, M. (2001). The quasi-biennial oscillation. *Reviews of Geophysics*, *39*, 179–229. https://doi.org/10.1029/1999RG000073

Barnston, A., & Livezey, R. (1987). Classification, seasonality and persistence of low-frequency atmospheric circulation patterns. *Monthly Weather Review*, *115*(6), 1083–1126. https://doi.org/10.1175/1520-0493(1987)115%3C1083:CSAPOL%3E2.0.CO;2

Bosilovich, M., Akella, S., Coy, L., Cullather, R., Draper, C., Gelaro, R., … Suarez, M. (2015). MERRA-2: Initial evaluation of the climate. NASA/TM–2015-104606/Vol. 43, NASA Technical Report Series on Global Modeling and Data Assimilation (p. 139). Retrieved from http://doi.org/NASA/TM%E2%80%932015-104606/Vol

Bosilovich, M. G., Robertson, F. R., & Chen, J. (2011). Global energy and water budgets in MERRA. *Journal of Climate*, *24*(22), 5721–5739. https://doi.org/10.1175/2011JCLI4175.1

Coleman, J. S. M., & Rogers, J. C. (2003). Ohio River valley winter moisture conditions associated with the Pacific–North American teleconnection pattern. *Journal of Climate*, *16*(6), 969–981.

Cordeira, J. M., Ralph, F. M., & Moore, B. J. (2013). The development and evolution of two atmospheric rivers in proximity to western North Pacific tropical cyclones in October 2010. *Monthly Weather Review*, *141*, 4234–4255. https://doi.org/10.1175/MWR-D-13-00019.1

Dettinger, M. (2011). Climate change, atmospheric rivers, and floods in California—A multimodel analysis of storm frequency and magnitude changes. *Journal of the American Water Resources Association*, *47*(3), 514–523. https://doi.org/10.1111/j.1752-1688.2011.00546.x

Dettinger, M. D. (2013). Atmospheric rivers as drought busters on the U.S. West Coast. *Journal of Hydrometeorology*, *14*(6), 1721–1732. https://doi.org/10.1175/JHM-D-13-02.1

Dettinger, M. D., Ralph, F. M., Das, T., Neiman, P. J., & Cayan, D. R. (2011). Atmospheric rivers, floods and the water resources of California. *Water*, *3*(4), 445–478. https://doi.org/10.3390/w3020445

Ebdon, R. A. (1960). Notes on the wind flow at 50 mb in tropical and sub-tropical regions in January 1957 and January 1958. *Quarterly Journal of the Royal Meteorological Society*, *86*(370), 540–542. https://doi.org/10.1002/qj.49708637011

Gan, M. A., & Rao, V. B. (1991). Surface cyclogenesis over South America. *Monthly Weather Review*, *119*(5), 1293–1302. https://doi.org/10.1175/1520-0493(1991)119%3C1293:SCOSA%3E2.0.CO;2

Gelaro, R., McCarty, W., Suárez, M. J., Todling, R., Molod, A., Takacs, L., … Zhao, B. (2017). The Modern-Era Retrospective Analysis for Research and Applications, Version 2 (MERRA-2). *Journal of Climate*, *30*(14), 5419–5454. https://doi.org/10.1175/JCLI-D-16-0758.1

Gorodetskaya, I. V., Tsukernik, M., Claes, K., Ralph, M. F., Neff, W. D., & Van Lipzig, N. P. M. (2014). The role of atmospheric rivers in anomalous snow accumulation in East Antarctica. *Geophysical Research Letters*, *41*, 6199–6206. https://doi.org/10.1002/2014GL060881

Guan, B., Molotch, N. P., Waliser, D. E., Fetzer, E. J., & Neiman, P. J. (2010). Extreme snowfall events linked to atmospheric rivers and surface air temperature via satellite measurements. *Geophysical Research Letters*, *37*, L20401. https://doi.org/10.1029/2010GL044696

Guan, B., & Waliser, D. E. (2015). Detection of atmospheric rivers: Evaluation and application of an algorithm for global studies. *Journal of Geophysical Research: Atmospheres*, *120*, 12,514–12,535. https://doi.org/10.1002/2015JD024257

Guan, B., Waliser, D. E., Molotch, N. P., Fetzer, E. J., & Neiman, P. J. (2012). Does the Madden–Julian Oscillation influence wintertime atmospheric rivers and snowpack in the Sierra Nevada? *Monthly Weather Review*, *140*(2), 325–342. https://doi.org/10.1175/MWR-D-11-00087.1

Hagos, S., Ruby Leung, L., Yang, Q., Zhao, C., & Lu, J. (2015). Resolution and dynamical core dependence of atmospheric river frequency in global model simulations. *Journal of Climate*, *28*(7), 2764–2776. https://doi.org/10.1175/JCLI-D-14-00567.1

Hodges, K. I. (1994). A general-method for tracking analysis and its application to meteorological data. *Monthly Weather Review*, *122*(11), 2573–2586. https://doi.org/10.1175/1520-0493(1994)122%3C2573:AGMFTA%3E2.0.CO;2

Hood, L. L. (2017). QBO/solar modulation of the boreal winter Madden-Julian oscillation: A prediction for the coming solar minimum. *Geophysical Research Letters*, *44*, 3849–3857. https://doi.org/10.1002/2017GL072832

Hoskins, B. J., & Hodges, K. I. (2005). A New Perspective on Southern Hemisphere Storm Tracks. *Journal of Climate*, *18*, 4108–4129. https://doi.org/10.1175/JCLI3570.1

Jiang, T., Evans, K. J., Deng, Y., & Dong, X. (2014). Intermediate frequency atmospheric disturbances: A dynamical bridge connecting western U.S. extreme precipitation with East Asian cold surges. *Journal of Geophysical Research: Atmospheres*, *119*, 3723–3735. https://doi.org/10.1002/2013JD021209

Jeong, J.-H., & Ho, C.-H. (2005). Changes in occurrence of cold surges over East Asia in association with Arctic Oscillation. *Geophysical Research Letters*, *32*, L14704. https://doi.org/10.1029/2005GL023024

Jones, S. C., Harr, P. a., Abraham, J., Bosart, L. F., Bowyer, P. J., Evans, J. L., & Thorncroft, C. (2003). The extratropical transition of tropical cyclones: Forecast challenges, current understanding, and future directions. *Weather and Forecasting*, *18*(6), 1052–1092. https://doi.org/10.1175/1520-0434(2003)018%3C1052:TETOTC%3E2.0.CO;2

Kerns, B., & Zipser, E. (2008). Four years of tropical ERA-40 vorticity maxima tracks. Part I: Climatology and vertical vorticity structure. *Monthly Weather Review*, *136*(11), 4301–4319. https://doi.org/10.1175/2008MWR2390.1

Kerns, B., & Zipser, E. (2009). Four years of tropical ERA-40 vorticity maxima tracks. Part II: Differences between developing and nondeveloping disturbances. *Monthly Weather Review*, *137*(8), 2576–2591. https://doi.org/10.1175/2008MWR2545.1

Latif, M., & Barnett, T. P. (1994). Causes of decadal climate variability over the North Pacific and North America. *Science*, *266*(5185), 634–637. https://doi.org/10.1126/science.266.5185.634

Lavers, D. A., & Villarini, G. (2013). Atmospheric rivers and flooding over the central United States. *Journal of Climate*, *26*(20), 7829–7836. https://doi.org/10.1175/JCLI-D-13-00212.1

Lavers, D. A., Villarini, G., Allan, R. P., Wood, E. F., & Wade, A. J. (2012). The detection of atmospheric rivers in atmospheric reanalyses and their links to British winter floods and the large-scale climatic circulation. *Journal of Geophysical Research*, *117*, D20106. https://doi.org/10.1029/2012JD018027

Lavers, D. A., Richard, P. A., Villarini, G., Benjamin, L. H., David, J. B., & Andrew, J. W. (2013). Future changes in atmospheric rivers and their implications for winter flooding in Britain. *Environmental Research Letters*, *8*, 034010. https://doi.org/10.1088/1748-9326/8/3/034010

Leathers, D. J., Yarnal, B., Palecki, M. A., Leathers, D. J., Yarnal, B., & Palecki, M. A. (1991). The Pacific/North American teleconnection pattern and United States climate. Part I: Regional temperature and precipitation associations. *Journal of Climate*, *4*(5), 517–528. https://doi.org/10.1175/1520-0442(1991)004%3C0517:TPATPA%3E2.0.CO;2

Lindzen, R. S., & Holton, J. R. (1968). A theory of the quasi-biennial oscillation. *Journal of the Atmospheric Sciences*, *25*(6), 1095–1107. https://doi.org/10.1175/1520-0469(1968)025%3C1095:ATOTQB%3E2.0.CO;2

Lorenz, E. N. (1951). Seasonal and irregular variations of the Northern Hemisphere sea-level pressure profile. *Journal of Meteorology*, *8*(1), 52–59. https://doi.org/10.1175/1520-0469(1951)008%3C0052:SAIVOT%3E2.0.CO;2

Moore, B. J., Neiman, P. J., Ralph, F. M., & Barthold, F. E. (2012). Physical processes associated with heavy flooding rainfall in Nashville, Tennessee, and vicinity during 1–2 May 2010: The role of an atmospheric river and mesoscale convective systems. *Monthly Weather Review*, *140*(2), 358–378. https://doi.org/10.1175/MWR-D-11-00126.1

Mundhenk, B. D., Barnes, E. A., & Maloney, E. D. (2016). All-season climatology and variability of atmospheric river frequencies over the North Pacific. *Journal of Climate*, *29*(13), 4885–4903. https://doi.org/10.1175/JCLI-D-15-0655.1

Neff, W., Compo, G. P., Ralph, F. M., & Shupe, M. D. (2014). Continental heat anomalies and the extreme melting of the Greenland ice surface in 2012 and 1889. *Journal of Geophysical Research*, *119*, 6520–6536. https://doi.org/10.1002/2014JD021470

Neiman, P. J., Gottas, D. J., White, A. B., Gutman, S. I., & Ralph, F. M. (2009). A water vapour flux tool for precipitation forecasting. *Proceedings of the ICE - Water Management*, *162*(2), 83–94. https://doi.org/10.1680/wama.2009.162.2.83

Neiman, P. J., Ralph, F. M., Moore, B. J., Hughes, M., Mahoney, K. M., Cordeira, J. M., & Dettinger, M. D. (2013). The landfall and inland penetration of a flood-producing atmospheric river in Arizona. Part I: Observed synoptic-scale, orographic, and hydrometeorological characteristics. *Journal of Hydrometeorology*, *14*(2), 460–484. https://doi.org/10.1175/JHM-D-12-0101.1

Neiman, P. J., Ralph, F. M., Wick, G. a., Lundquist, J. D., & Dettinger, M. D. (2008). Meteorological characteristics and overland precipitation impacts of atmospheric rivers affecting the west coast of North America based on eight years of SSM/I satellite observations. *Journal of Hydrometeorology*, *9*(1), 22–47. https://doi.org/10.1175/2007JHM855.1

Nguyen, H., Hendon, H. H., Lim, E.-P., Boschat, G., Maloney, E., & Timbal, B. (2017). Variability of the extent of the Hadley circulation in the southern hemisphere: A regional perspective. *Climate Dynamics*. https://doi.org/10.1007/s00382-017-3592-2

Nguyen, P., Sorooshian, S., Thorstensen, A., Tran, H., Huynh, P., Pham, T., … Braithwaite, D. (2017). Exploring trends through "rainsphere": Research data transformed into public knowledge. *Bulletin of the American Meteorological Society*, *98*(4), 653–658. https://doi.org/10.1175/BAMS-D-16-0036.1

iRain-UC Irvine (2017). iRain (2.1.2) [Mobile application software]. Retrieved from http://itunes.apple.com

Ralph, F. M., Coleman, T., Neiman, P. J., Zamora, R. J., & Dettinger, M. D. (2012). Observed impacts of duration and seasonality of atmospheric-river landfalls on soil moisture and runoff in coastal northern California. *Journal of Hydrometeorology*, *14*(2), 443–459. https://doi.org/10.1175/JHM-D-12-076.1

Ralph, F. M., & Dettinger, M. D. (2011). Storms, floods, and the science of atmospheric rivers. *Eos, Transactions American Geophysical Union*, *92*(32), 265–266. https://doi.org/10.1029/2011EO320001

Ralph, F. M., Neiman, P. J., Kiladis, G. N., Weickmann, K., & Reynolds, D. W. (2011). A multiscale observational case study of a Pacific atmospheric River exhibiting tropical–extratropical connections and a mesoscale frontal wave. *Monthly Weather Review*, *139*(4), 1169–1189. https://doi.org/10.1175/2010MWR3596.1

Ralph, F. M., Neiman, P. J., & Wick, G. A. (2004). Satellite and CALJET aircraft observations of atmospheric rivers over the eastern North Pacific Ocean during the winter of 1997/98. *Monthly Weather Review*, *132*(7), 1721–1745. https://doi.org/10.1175/1520-0493(2004)132%3C1721:SACAOO%3E2.0.CO;2

Ralph, F. M., Neiman, P. J., Wick, G. A., Gutman, S. I., Dettinger, M. D., Cayan, D. R., & White, A. B. (2006). Flooding on California's Russian River: Role of atmospheric rivers. *Geophysical Research Letters*, *33*, L13801. https://doi.org/10.1029/2006GL026689

Ramos, A. M., Nieto, R., Tome, R., Gimeno, L., Trigo, R. M., Liberato, M. L. R., & Lavers, D. A. (2016). Atmospheric rivers moisture sources from a Lagrangian perspective. *Earth System Dynamics*, *7*(2), 371–384. https://doi.org/10.5194/esd-7-371-2016

Rienecker, M. M., Suarez, M. J., Gelaro, R., Todling, R., Bacmeister, J., Liu, E., … Woollen, J. (2011). MERRA: NASA's Modern-Era Retrospective Analysis for Research and Applications. *Journal of Climate*, *24*(14), 3624–3648. https://doi.org/10.1175/JCLI-D-11-00015.1

Ruby Leung, L., & Qian, Y. (2009). Atmospheric rivers induced heavy precipitation and flooding in the western U.S. simulated by the WRF regional climate model. *Geophysical Research Letters*, *36*, L03820. https://doi.org/10.1029/2008GL036445

Rutz, J. J., Steenburgh, W. J., & Ralph, F. M. (2014). Climatological characteristics of atmospheric rivers and their inland penetration over the western United States. *Monthly Weather Review*, *142*(2), 905–921. https://doi.org/10.1175/MWR-D-13-00168.1

Schultz, D. M., Bracken, W. E., Bosart, L. F., Hakim, G. J., Bedrick, M. A., Dickinson, M. J., & Tyle, K. R. (1997). The 1993 superstorm cold surge: Frontal structure, gap flow, and tropical impact. *Monthly Weather Review*, *125*(1), 5–39. https://doi.org/10.1175/1520-0493(1997)125%3C0005:TSCSFS%3E2.0.CO;2

Sellars, S., Gao, X., & Sorooshain, S. (2015). An object-oriented approach to investigating the impact of climate variability on precipitation: A western United States case study. *Journal of Hydrometeorology*, *16*(2), 830–842. https://doi.org/10.1175/JHM-D-14-0101.1

Sellars, S., Nguyen, P., Chu, W., Gao, X., Hsu, K., & Sorooshian, S. (2013). Computational Earth science: Big data transformed into insight. *Eos, Transactions American Geophysical Union*, *94*(32), 277–278. https://doi.org/10.1002/2013EO320001

Sellars, S. L., Nguyen, P., & Kawzenuk, B. (2017). The CONNected objeECT, or CONNECT algorithm applied to National Aeronautics and Space Administration (NASA) Modern-Era Retrospective Analysis for Research and Applications, version 2 (MERRA V2) - integrated water vapor from 1980 to 2016. UC San Diego Library Digital Collections. https://doi.org/10.6075/J01834P8

Son, S., Lim, Y., Yoo, C., Hendon, H. H., & Kim, J. (2017). Stratospheric control of the Madden–Julian Oscillation. *Journal of Climate*, *30*(6), 1909–1922. https://doi.org/10.1175/JCLI-D-16-0620.1

Steenburgh, W. J., Schultz, D. M., & Colle, B. A. (1998). The structure and evolution of gap outflow over the Gulf of Tehuantepec, Mexico. *Monthly Weather Review*, *126*(10), 2673–2691. https://doi.org/10.1175/1520-0493(1998)126%3C2673:TSAEOG%3E2.0.CO;2

Thompson, D. W. J., & Wallace, J. M. (1998). The Arctic oscillation signature in the wintertime geopotential height and temperature fields. *Geophysical Research Letters*, *25*, 1297–1300. https://doi.org/10.1029/98GL00950

Thompson, D. W. J., & Wallace, J. M. (2000a). Annular modes in the extratropical ciculation. Part 1: Month-to-month variability. *Journal of Climate*, *13*(5), 1000–1016. https://doi.org/10.1175/1520-0442(2000)013%3C1000:AMITEC%3E2.0.CO;2

Thompson, D. W. J., & Wallace, J. M. (2000b). Annular modes in the extratropical circulation. Part II: Trends. *Journal of Climate*, *13*(5), 1018–1036. https://doi.org/10.1175/1520-0442(2000)013%3C1018:AMITEC%3E2.0.CO;2

Ullrich, P., & Zarzycki, C. (2017). TempestExtremes: A framework for scale-insensitive pointwise feature tracking on unstructured grids. *Geoscientific Model Development*, *10*(3), 1069–1090. https://doi.org/10.5194/gmd-10-1069-2017

Vera, C. S., Vigliarolo, P. K., & Berbery, E. H. (2002). Cold season synoptic-scale waves over subtropical South America. *Monthly Weather Review*, *130*(3), 684–699. https://doi.org/10.1175/1520-0493(2002)130%3C0684:CSSSWO%3E2.0.CO;2

Viale, M., Houze, R. A., & Rasmussen, K. L. (2013). Upstream orographic enhancement of a narrow cold-frontal rainband approaching the Andes. *Monthly Weather Review*, *141*(5), 1708–1730. https://doi.org/10.1175/MWR-D-12-00138.1

Viale, M., & Nuñez, M. N. (2011). Climatology of winter orographic precipitation over the subtropical central Andes and associated synoptic and regional characteristics. *Journal of Hydrometeorology*, *12*(4), 481–507. https://doi.org/10.1175/2010JHM1284.1

Waliser, D., & Guan, B. (2017). Extreme winds and precipitation during landfall of atmospheric rivers. *Nature Geoscience*, *10*(3), 179–183. https://doi.org/10.1038/ngeo2894

White, A. B., Anderson, M. L., Dettinger, M. D., Ralph, F. M., Hinojosa, A., Cayan, D. R., … Coleman, T. (2013). A twenty-first-century California observing network for monitoring extreme weather events. *Journal of Atmospheric and Oceanic Technology*, *30*(8), 1585–1603. https://doi.org/10.1175/JTECH-D-12-00217.1

Wick, G. A., Neiman, P. J., & Ralph, F. M. (2013). Description and validation of an automated objective technique for identification and characterization of the integrated water vapor signature of atmospheric rivers. *IEEE Transactions on Geoscience and Remote Sensing*, *51*(4), 2166–2176. https://doi.org/10.1109/TGRS.2012.2211024

Zhu, Y., & Newell, R. E. (1994). Atmospheric rivers and bombs. *Geophysical Research Letters*, *21*, 1999–2002. https://doi.org/10.1029/94GL01710

Zhu, Y., & Newell, R. (1998). A proposed algorithm for moisture fluxes from atmospheric rivers. *Monthly Weather Review*, *13*(3), 725–735.